analytical chemistry

Article

Cite This: *Anal. Chem.* 2018, 90, 13096−13103

pubs.acs.org/ac

High-Throughput Enzyme Kinetics with 3D Microfluidics and Imaging SAMDI Mass Spectrometry

Jennifer Grant,[†] Sohrab Habibi Goudarzi,[‡,∥] and Milan Mrksich*[,†,§]

[†]Department of Chemistry, [‡]Integrated Molecular Structure Education and Research Center, [§]Department of Biomedical Engineering, Northwestern University, Evanston, Illinois 60208, United States

Supporting Information

ABSTRACT: Microfluidic systems are important for performing precise reagent manipulations and reducing material consumption in biological assays. However, optical detection methods limit analyses to fluorescent or UV-active compounds and traditional 2D fluidic designs have limited degrees of freedom. This article describes a microfluidic device that has three inputs and performs 2592 distinct enzyme reactions using only 150 μL of reagent with quantitative characterization. This article also introduces imaging self-assembled monolayers for matrix-assisted laser desorption/ionization mass spectrometry (iSAMDI-MS) to map reaction progress, by immobilization of the product onto the floor of the microfluidic channel, into an image that is used for calculating the Michaelis constant (K_m). This approach expands the scope of imaging mass spectrometry, microfluidic detection strategies, and the design of high-throughput reaction systems.

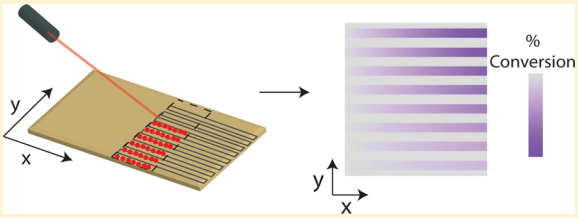

Microfluidic systems have been important for increasing the throughput of biological assays and reducing reagent consumption. For example, a microfluidic device for chromatin immunoprecipitation (ChIP) required only 100 cells and 700 nL of reagent for epigenomic studies of hematopoietic stem and progenitor cells.[1] In addition, octanol-assisted liposome assembly (OLA) enabled the on-chip production of biocompatible liposomes at rates exceeding 10 Hz using 10 μL of reagent.[2] However, the two-dimensional (2D) structure of most microfluidic devices is not well-suited for mixing multiple reagents in large numbers of combinations, and the need for fluorescent labels to analyze reaction products limits the generality of microfluidic formats for characterizing enzymes. Additionally, microfluidic devices are often designed with networks of valves and arrayed reaction chambers that add complexity to the device design and operation. In this article, we demonstrate the combination of a simple three-dimensional (3D) fluidic structure and imaging mass spectrometry (IMS) to perform 2592 unique biochemical experiments on a chip, and we highlight its applicability toward providing kinetic constants for an enzyme.

High-throughput microfluidic reaction systems can overcome the limitations inherent to manually preparing and analyzing thousands of separate experiments on the laboratory bench. For example, combinatorial microfluidic mixers based on a 3D network of channels have eliminated the need to manually mix and dispense solutions for large-scale biological screens.[3,4] In a landmark article, Quake and co-workers described a device having 1000 valve-controlled reaction chambers to rapidly access thousands of reaction conditions,[5] highlighting the advantages of using microfluidics for high-throughput screening applications. To circumvent the need for large numbers of integrated valves on a chip, Ismagilov and co-workers developed a droplet-based method to screen multiple reaction conditions for protein crystallization[6] and bacterial susceptibility to antibiotics.[7] That method has been integrated with a variety of detection methods, including MALDI mass spectrometry, to calculate the relative concentration of a reaction product.[8] These approaches demonstrate the potential of combining microfluidic devices with new detection strategies to enable high throughput experiments for a broad range of enzyme activities, while requiring substantially less reagent and shorter assay times than conventional approaches.

In this article, we present a method called imaging self-assembled monolayers for matrix-assisted laser desorption/ionization mass spectrometry (iSAMDI-MS) to obtain quantitative, high-throughput maps of reaction progress. We used iSAMDI-MS to quantitate 2592 unique experiments performed in flow, using only 150 μL of reagent, where the products were captured onto a self-assembled monolayer that could then be imaged with mass spectrometry to demonstrate its application toward calculating the Michaelis constant (K_m) of an enzyme−substrate reaction. We used a multilayer microfluidic device that generated a gradient of substrate concentration and simultaneously introduced an enzyme solution to each channel to initiate the reactions. As the reaction proceeded, the product underwent immobilization to a monolayer on the floor of the channel to record a kinetic profile of the reaction. We imaged the floor of the microfluidic device with SAMDI mass spectrometry to generate a 110 × 91 pixel array of adjacent 200 μm × 200 μm regions, and present

Received: September 25, 2018
Accepted: September 26, 2018
Published: September 26, 2018

DOI: 10.1021/acs.analchem.8b04391
Anal. Chem. 2018, 90, 13096−13103

a quantitative map of reaction progress. In this way, the device carried out thousands of reactions without requiring any valves or isolated reaction chambers. iSAMDI-MS is a powerful method that uses a simple fluidic device and a minimal amount of reagent to obtain a high-density data set of reaction progress.

MATERIALS AND METHODS

Buffers. All measurements were conducted in 0.1 M potassium phosphate buffer (pH 7.5).

Self-Assembled Monolayer Preparation. Standard glass microscope slides were cleaned using ethanol and water in a sonication bath. An electron beam evaporator (Thermionics VE-100) was used to deposit 5 nm Ti (0.02 nm s^{-1}) followed by 30 nm Au (0.05 nm s^{-1}) at a pressure between 1×10^{-6} and 8×10^{-6} Torr. The slides were soaked overnight at 25 °C in an ethanolic solution (0.5 mM total disulfide concentration) having a 2:3 ratio of an asymmetric disulfide terminated with a maleimide group and tri(ethylene glycol) group to a symmetric disulfide terminated with tri(ethylene glycol) groups. The slides were then rinsed with ethanol and water.

Microfluidic Device Fabrication. Poly(dimethylsiloxane) (PDMS) masters were rendered on SolidWorks software (Figure S1, Supporting Information). The master for the top layer had one 800 μm inlet branching into eight 250 μm width and 250 μm height channels. The master for the bottom layer had two 800 μm inlets that split and merged into eight 250 μm width and 250 μm height channels. The 800 μm width and 3 mm tall posts connected the bottom layer to the top layer, and the channels expanded to a width of 550 μm and height of 550 μm after this intersection. The files were converted to stl format and printed in a digital printing mode using a Stratasys Connex 350 3D printer in VeroWhite material (Stratasys Direct) with a glossy finish. The 3D printed masters were prepared for PDMS polymerization as previously described.[9] PDMS prepolymer mixture was mixed in a 1:10 ratio (w/w curing agent to prepolymer), degassed in a vacuum desiccator for 15 min, and poured into the 3D printed master. The master containing PDMS was degassed in a vacuum desiccator for 15 min and placed in a 43 °C oven overnight. The PDMS blocks were then peeled off of the mold and treated in a 130 °C oven for 10 min. The 3D-printed molds were reused for additional PDMS curing cycles. A 0.8 mm biopsy punch was used to form the inlets of the top and bottom PDMS layers, and to ensure that all of the through-holes in the bottom layer were completely formed. To ensure that the punched holes in the top layer intersected with the bottom layer, the two layers were aligned under a stereo microscope (Leica M125) before forming the inlets in the top layer. The top and bottom PDMS layers were then treated with 50 W air plasma for 35 s at 200 mTorr (Solarus Plasma Cleaner, Gatan, Inc.) and aligned under a stereo microscope. The two-layer PDMS device was placed onto the Au slide functionalized with the self-assembled monolayer so that the bottom PDMS layer was in contact with the slide. The PDMS and Au slide assembly was held together using light pressure from an external clamp made from extruded polycarbonate secured with six screws. The clamp had three 1.5 mm diameter holes to match the location of the three device inlets. PTFE tubing (0.042″ outer diameter, Cole-Parmer) was inserted into each inlet via stainless steel catheter couplers (22 ga × 15 mm, Instech), and the bottom layer was primed with buffer using a syringe pump (PhD 2000, Harvard Apparatus). The top layer was primed with buffer using a second syringe pump. Any remaining bubbles were removed by individually applying flow rates >500 μL min^{-1} to each syringe. The absence of bubbles was confirmed using a stereo microscope.

Microfluidic Device Calibration. Buffer was introduced into the top layer at a flow rate of 0.8 μL min^{-1}. Simultaneously, a solution of 350 μM L-glutathione reduced (≥98%, Sigma-Aldrich) and 350 μM [$^{13}C_2$,^{15}N]-GSH (≥ 95% purity; glycine-$^{13}C_2$, ≥ 98%; ^{15}N, 96−99%; ≥ 90% net peptide, Cambridge Isotope Laboratories, Inc.) was injected into one inlet of the bottom layer, and a solution of [$^{13}C_2$,^{15}N]-GSH (350 μM) was injected into the second inlet of the bottom layer at a flow rate of 0.4 μL min^{-1}. The device diluted GSH into a linear gradient of 8 concentrations, while maintaining the concentration of [$^{13}C_2$,^{15}N]-GSH. After 1 h, the device was rinsed by flowing the buffer into all three inlets for 5 min at 20 μL min^{-1}. The clamp was disassembled, the PDMS layers were peeled off of the chip, and the chip was rinsed with ethanol, water, and acetone. A solution of 2′,4′,6′-trihydroxyacetophenone monohydrate (THAP; ≥ 99.5%, Sigma-Aldrich) in acetone (25 mg mL^{-1}, 80 μL) was pipetted onto the chip. We found that the matrix crystallized more densely on the area of the monolayer in contact with the microfluidic channels, which allowed us to easily locate all 8 channels using the video camera on the MALDI TOF instrument (Autoflex III, Bruker Daltonics). iSAMDI-MS spectra were acquired in reflector positive mode using a mass range of 600−3000 m/z. The smartbeam-II laser was operated at 200 Hz with 125 laser pulses applied per spot using the "medium" aperture setting. The $[M + Na^+]^+$ adducts of the GSH-alkanedisulfide and [$^{13}C_2$, ^{15}N]-GSH-alkanedisulfide were extracted using flexAnalysis software (Bruker Daltonics). The % conversion was calculated using the monoisotopic peak intensity of GSH (I_{GSH}) and the monoisotopic peak intensity of [$^{13}C_2$,^{15}N]-GSH ($I_{[^{13}C_2,^{15}N]\text{-GSH}}$), and it is plotted in Figure S2, Supporting Information.

$$\%\text{Conversion} = 100 \times \frac{I_{GSH}}{I_{GSH} + I_{[^{13}C_2,^{15}N]\text{-GSH}}} \quad (1)$$

The response follows a linear dilution profile, demonstrating that the bottom layer generates a serial dilution, and that calculating the % conversion from the extracted $[M + Na^+]^+$ adducts is quantitative.

Microfluidic Experiments for Determining K_m. Buffer was introduced into the top layer at 0.8 μL min^{-1}. Simultaneously, a solution of oxidized glutathione (350 μM, ≥ 98%, Sigma) was injected into one inlet of the bottom layer, and buffer was injected into the other inlet of the bottom layer at a flow rate of 0.4 μL min^{-1}. The device was operated for 25 min to equilibrate the flows. The top layer inlet was immediately replaced with a solution of NADPH (200 μM, ≥ 97%, Roche), [$^{13}C_2$,^{15}N]-GSH (350 μM), and human glutathione reductase (865 nM, Sigma), and the solution flowed at 0.8 μL min^{-1}. The flow rate into both inlets of the bottom layer was kept at 0.4 μL min^{-1}. The device was operated for 1 h. The clamp was disassembled; the PDMS layers were peeled off of the chip; and the chip was rinsed with ethanol, water, and acetone.

Mass Spectrometry Imaging. Matrix (25 mg mL^{-1} THAP in acetone) was applied by pipetting (80 μL) on top of the slide and letting the matrix solution fall to the base of the slide. A 22.0 × 18.2 mm region of interest (ROI) was selected

DOI: 10.1021/acs.analchem.8b04391
Anal. Chem. 2018, 90, 13096−13103

using FlexImaging software (Bruker Daltonics). MALDI-IMS was acquired by creating an AutoXecute method as previously described.[10] Spectra were acquired with a 200 μm lateral resolution and with 125 laser shots accumulated per pixel using the "medium" aperture setting. The laser pulse rate was 200 Hz, and spectra were obtained with a mass window of 600−3000 m/z.

Image Analysis and Quantitation. Ion intensity maps were generated on FlexImaging software at 1183.2 ± 0.2, 1180.2 ± 0.2, and 873.2 ± 0.2 Da, corresponding to the [$^{13}C_2$,^{15}N]-GSH-alkanedisulfide, GSH-alkanedisulfide, and maleimide-alkanedisulfide conjugate, respectively. The mis file was converted to an imzML using FlexImaging software and imported into MSiReader v1.00. A 108 × 88 pixel region downstream of the top and bottom layer junction was selected on MSiReader. Peak intensities of 1180.2 ± 0.2 and 1183.2 ± 0.2 Da were exported into Excel, and the % conversion was determined using eq 1. Three to four rows of pixels in each channel contained GSH and [$^{13}C_2$,^{15}N]-GSH bound to the self-assembled monolayer. The space between the channels did not have any bound analyte, and the conversion in these locations were set to zero. A rectangular 108 × 88 pixel array reporting the % conversion was plotted in a heatmap (MATLAB R2016a). The flow velocity was determined using $Q = AV$, where Q is the volumetric flow rate, and A is the cross-sectional area of the channel. The amount of time required for the fluid to flow downstream across each 200 μm pixel was calculated and plotted against the % conversion. Linear regression was used to determine the slope of each plot, and the three replicates from each channel were averaged to obtain V_0. The initial velocities were plotted as a function of GSSG concentration and fitted to the Michalis−Menten model (Enzyme Kinetics Module, SigmaPlot 12.0, Systat Software).

Ablation Spot Diameter Determination. The microfluidic device was operated with hGR, GSSG, NADPH, and [$^{13}C_2$,^{15}N]-GSH. MALDI-IMS was acquired as previously described. The diameter of 80 ablation spots were recorded using a stereozoom microscope (Nikon SMZ1500) and NIS-Elements D 3.0 software (Nikon).

RESULTS

Experimental Design. Our device for measuring the Michaelis constant for an enzyme is shown in Figure 1. The device has three input solutions, enzyme, substrate, and buffer, and two layers of channels on top of a substrate functionalized with a self-assembled monolayer. The bottom layer uses controlled diffusive mixing of the substrate and buffer to give a linear concentration gradient of substrate along eight parallel channels.[11,12] The top layer partitions a solution of enzyme and calibrant into a set of eight identical parallel channels that are then mixed with the substrate in the bottom layer to initiate the reactions. As the reactions flow down the channels in the bottom layer, the product of the reaction undergoes immobilization to a self-assembled monolayer on the floor of the channel. Hence, the position along the channel corresponds to the reaction time such that each channel has a full kinetic profile for each reaction and each channel contains a unique substrate concentration, thereby providing all of the information necessary to determine the K_m. We included a constant concentration of an isotopically labeled version of the product to quantitate the amount of product formed. The ratio of peak intensities for the product and calibrant gives the product yield in the solution where it

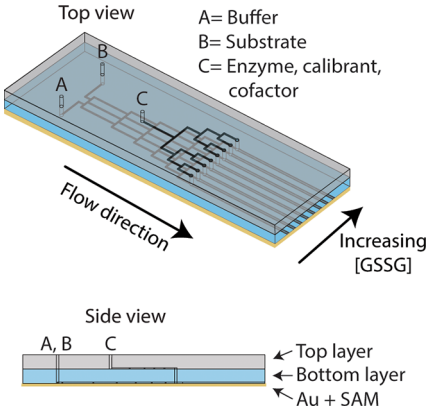

Figure 1. Inlets A (buffer) and B (substrate) deliver reagent into the bottom layer with unique concentrations of substrate in each of the eight final channels. Inlet C delivers enzyme into the top layer, which is then introduced into the bottom layer. Both layers are placed on top of a gold slide functionalized with a self-assembled monolayer terminated with maleimide functional groups.

underwent immobilization. The device was operated by flowing the three solutions into the device for approximately 1 h. The fluidic cassette was disassembled and iSAMDI-MS was used to quantitate the amount of product and calibrant with a resolution of 200 μm (square pixels) directly from the monolayer.

The monolayer comprising the floor of the microfluidic device was formed by self-assembly of maleimide-terminated disulfides and tri(ethylene glycol)-terminated disulfides on a gold-coated glass slide. The maleimide groups serve to immobilize cysteine-terminated peptides by a Michael addition of the thiol group and the tri(ethylene glycol) groups prevent nonspecific adsorption of the enzyme. Substantial work has shown that the monolayers are compatible with analysis by MALDI-TOF mass spectrometry (i.e., the SAMDI technique) and have been applied to analyzing a broad range of enzyme activities.[13−16]

In the present example, we use human glutathione reductase (hGR) which catalyzes the NADPH-dependent conversion of oxidized glutathione (GSSG) to reduced glutathione (GSH) (Figure 2A). The free thiol group in GSH allows the product of the reaction to be immobilized to the self-assembled monolayer, while the GSSG substrate lacks a free thiol group and is unable to undergo immobilization with the monolayer. We included an isotopically labeled GSH ([$^{13}C_2$,^{15}N]-GSH) at constant concentration in the reaction mixtures. This molecule underwent co-immobilization with the product and allows for quantitation of the product by calculating the ratio of peak intensities in the mass spectrum. We used an isotopomer of the actual product to ensure that both GSH and [$^{13}C_2$,^{15}N]-GSH have identical immobilization rates and ionization efficiencies in the mass spectrometry experiments. We validated the detection of hGR activity with SAMDI-MS by allowing a mixture of hGR, GSSG, [$^{13}C_2$,^{15}N]-GSH, and NADPH to react and pipetted the reaction mixture onto the self-assembled monolayer to allow immobilization of the product and calibrant. SAMDI-MS spectra were obtained from 125 laser shots with a fixed sample stage to simulate imaging acquisition conditions. A SAMDI-MS spectrum of the monolayer before the hGR-catalyzed reaction showed peaks at m/z 809, 841, and 873 corresponding to the maleimide-alkyldisulfide conjugate (Figure 2C). Treatment of the monolayer with the reaction

DOI: 10.1021/acs.analchem.8b04391
Anal. Chem. 2018, 90, 13096−13103

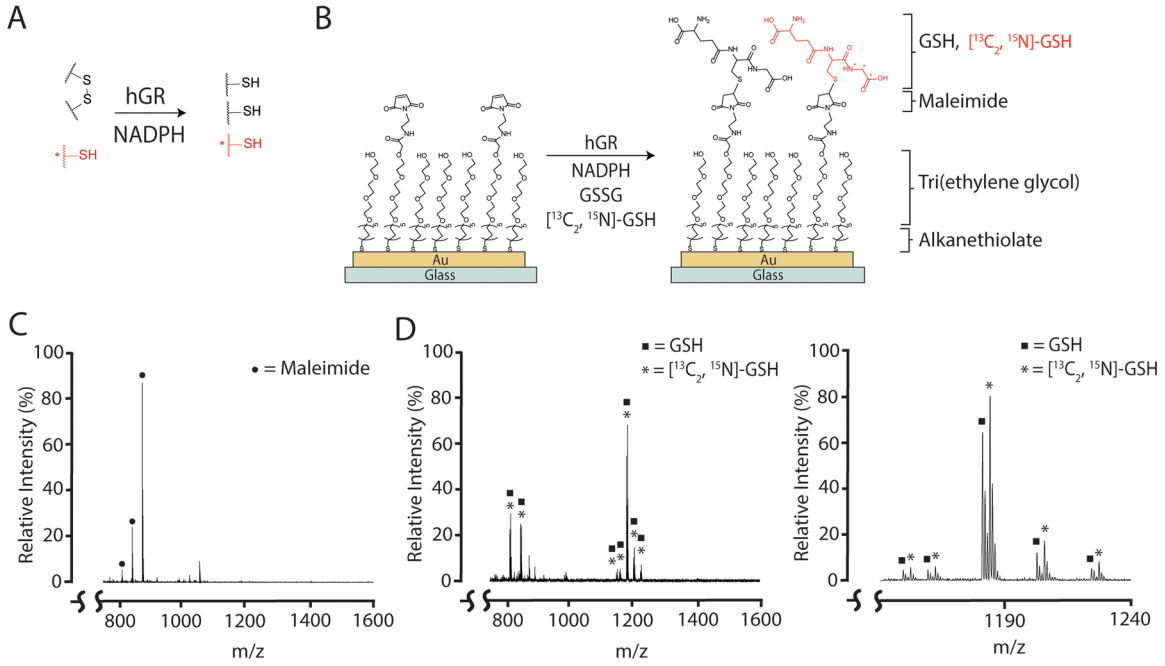

Figure 2. (A) hGR reaction. An isotope of reduced glutathione (red) is present for GSH quantitation. (B) GSH and [$^{13}C_2$,^{15}N]-GSH bind to a self-assembled monolayer terminated with maleimide functional groups that constitute the floor of the fluidic channel. (C) iSAMDI-MS spectrum with peaks at m/z 809.16, 841.19, and 873.12 (circles) representing the maleimide-alkyldisulfide conjugate. m/z range 750−1600. (D) iSAMDI-MS spectra from a channel after the hGR reaction. The GSH-alkyldisulfide conjugate and GSH-alkanethiol conjugate peaks are noted by squares at m/z = 812.08, 846.09, 1148.21, 1180.24, 1202.18, and 1224.23. Peaks representing the [$^{13}C_2$,^{15}N]-GSH-alkyldisulfide conjugate and [$^{13}C_2$,^{15}N]-GSH-alkanethiol conjugate are represented by asterisks (m/z = 815.09, 849.09, 1151.33, 1183.25, 1205.20, 1227.14). Spectra were accumulated with 125 laser pulses. Peaks representing the maleimide-alkyldisulfide conjugate are no longer present. (Left) m/z range 750−1600; (right) m/z range 1140−1240. Peak assignments are provided in Table S1, Supporting Information.

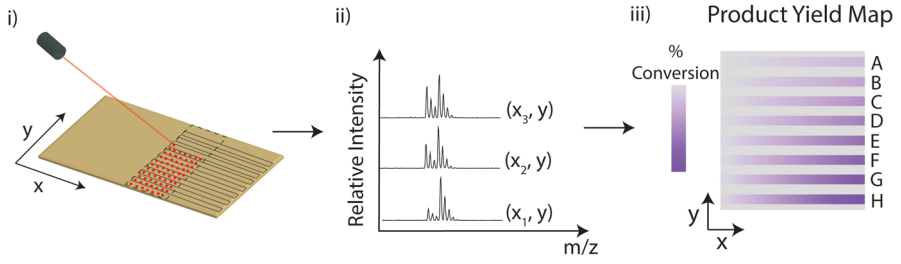

Figure 3. (i) A MALDI-IMS laser ablates pixels with a ROI at a lateral resolution of 200 μm. (ii) iSAMDI-MS spectra are accumulated at each x,y-coordinate. (iii) Imaging data is imported into the MSiReader[23,24] for peak intensity extraction. A heatmap of conversion at each x,y-coordinate is obtained from the extracted data (theoretical heatmap shown).

mixture revealed peaks representing the GSH-akyldisulfide conjugate and the [$^{13}C_2$,^{15}N]-GSH-alkyldisulfide conjugate (Figure 2D).

The top and bottom PDMS layers were each prepared by casting against a 3D printed master (Figure S1, Supporting Information). The use of a 3D printer to prepare the masters was significant because it increased the rate at which designs could be iteratively tested. The master for the bottom layer contained a 2-input/8-output pyramidal network of 250 μm tall, 250 μm wide channels that split and combined with neighboring streams at each node. Cylindrical posts (3 mm tall, 800 μm diameter) were placed at each output of the pyramidal network to generate through-holes for connecting the two PDMS layers. The eight channels downstream of the cylindrical posts were 550 μm wide and 550 μm tall, allowing for the acquisition of three technical replicate kinetic traces. The top layer contained a 1-input/8-output network of channels 250 μm wide and 250 μm tall. The 3D-printed masters allowed for facile PDMS polymerization and removal, and the masters were used for subsequent polymerization cycles.

Device Operation. The device operation began with aligning both PDMS layers onto a gold-coated substrate functionalized with the self-assembled monolayer (Figure S3, Supporting Information). The PDMS and monolayer assembly were held together using light pressure from an external clamp. To generate the substrate gradient, potassium phosphate buffer and GSSG were flowed into both inlets A and B of the bottom layer, respectively, and potassium phosphate buffer was flowed into the top layer for 25 min to equilibrate the device. The inlet of the top layer was then replaced with a solution of hGR, [$^{13}C_2$,^{15}N]-GSH, and NADPH to initiate the reactions, which were allowed to flow for 1 h. During this time, the product and calibrant underwent immobilization to the monolayer and once all of the maleimide groups had reacted, the reaction kinetics were permanently recorded on the monolayer. The

DOI: 10.1021/acs.analchem.8b04391
Anal. Chem. 2018, 90, 13096−13103

microfluidic device was then rinsed with potassium phosphate buffer and removed from the monolayer, which was then imaged with SAMDI mass spectrometry.

Matrix crystal homogeneity and spacing significantly affects the spectral quality and resolution in IMS workflows. With this in mind, we developed a simple matrix application technique for iSAMDI-MS that did not require matrix sprayers or precision injectors commonly implemented in IMS workflows.[17] Additionally, we confirmed that we could accumulate 125 shots within each 200 μm^2 region without any pixel overlap (Figure S4, Supporting Information).

Acquisition and Analysis. MALDI IMS has emerged as a powerful tool to determine the spatial distribution of small molecules,[18] metabolites,[19] peptides,[20,21] and proteins[10,22] from a 2D array of mass spectra. We combined the quantitative and high-throughput features of SAMDI-MS with the spatial resolution of microfluidics and IMS in a single experimental setup and workflow (Figure 3).

To begin iSAMDI-MS data acquisition, an image of the matrix-coated monolayer was scanned to identify the ROI. We selected an ROI that began at the junction between the top and bottom layers and extended along the direction of the fluid flow. The resulting ion maps of GSH, [$^{13}C_2$,^{15}N]-GSH, and maleimide correlated well with the channel features in the bottom layer (Figure 4). The ion maps revealed the

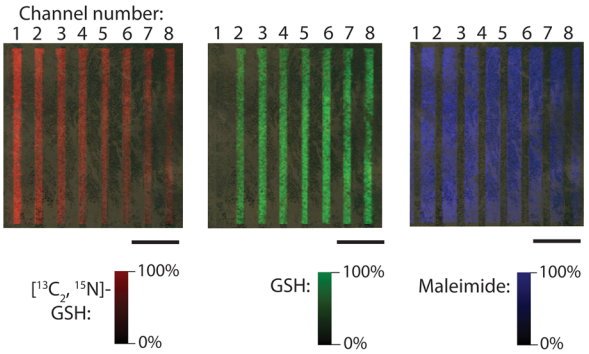

Figure 4. Ion maps of analyte detected with iSAMDI-MS (110 × 91 pixel array). (Left) Map of [$^{13}C_2$,^{15}N]-GSH-alkyldisulfide conjugate (m/z 1183.20) visualized in red. (Center) Map of GSH-alkyldisulfide conjugate (m/z 1180.20) visualized in green. (Right) Map of maleimide-alkyldisulfide conjugate (m/z 873.18) visualized in blue. Scale bar = 5 mm.

distribution of each analyte, and significantly, did not require prior spatial registration of the monolayer. The red color represents the distribution of [$^{13}C_2$,^{15}N]-GSH-alkyldisulfide conjugate ([M + Na]$^+$), the green color represents the GSH-alkyldisulfide conjugate ([M + Na]$^+$), and the blue color represents the maleimide-alkyldisufide conjugate ([M + Na]$^+$). The presence of [$^{13}C_2$,^{15}N]-GSH in each channel shows that hGR was successfully delivered into the bottom layer, because [$^{13}C_2$,^{15}N]-GSH and hGR were co-injected into the top layer. The maleimide distribution confirmed that the channels did not leak during the device operation. A plot of [$^{13}C_2$,^{15}N]-GSH-alkyldisulfide ([M + Na]$^+$) peak intensity at a fixed pixel on the x-axis showed that three to four pixels containing the ion were obtained across the 550 μm wide channels (Figure S5, Supporting Information). Therefore, three to four replicate kinetic profiles were acquired at each substrate concentration. SAMDI mass spectra representing one pixel from each channel are shown in Figure S6, Supporting Information.

To demonstrate the applicability of iSAMDI-MS for assaying enzyme kinetics, we calculated the product conversion and K_m of hGR. We extracted a 108 × 88 pixel array and calculated GSH yield from each pixel located on a channel. From 9504 pixels in the image, 2592 were located on a channel and used for GSH product quantitation. The spatial product distribution revealed differences in relative reaction velocities in accordance with Michaelis–Menten kinetics (Figure 5A).

The Michaelis–Menten constant, K_m, describes the effective affinity of an enzyme for its substrate, and it is one of the most important equations for describing enzyme activity. The K_m is calculated from the Michaelis–Menten equation

$$V_0 = \frac{V_{max}[S]}{K_m + [S]} \quad (2)$$

where V_0, V_{max}, and S are the initial reaction velocity, maximum reaction velocity, and the substrate concentration, respectively. We chose t = 0 to be the first point on the bottom layer that intersected with the top layer. The average fluid velocity was used to approximate the elapsed time from t = 0 to the first pixel in the ROI. The relative time for the fluid flow to travel 200 μm in the longitudinal direction was calculated using the average fluid velocity and plotted against product conversion (Figure 5B). In total, 24 unique initial velocity curves were obtained with 108 data points (pixels) each, and linear regression was used to fit each line with the slope representing V_0 (Figures 5B,C, and S7, Supporting Information). The three V_0 values from each channel were averaged and plotted as a function of substrate concentration (Figure 5D). Fitting this data to the Michaelis–Menten equation revealed a K_m of 52.2 ± 10.8 μM (SigmaPlot, Systat Software). Our K_m agrees well with the previously published value of 65 μM,[25−27] demonstrating the practicality and feasibility of this method.

DISCUSSION

This article demonstrates how iSAMDI-MS can be integrated with a simple microfluidic device to perform high-throughput biochemical experiments with quantitative characterization of enzyme kinetics. This work is significant because it illustrates how modest amounts of reagents can be combined to perform thousands of distinct reactions. The reaction density is achieved by covalently capturing the reaction product on a self-assembled monolayer to generate a spatial map of the reaction progress. The use of self-assembled monolayers as the floor of the microfluidic device allowed the selective immobilization of the product (with the isotopically labeled calibrant) and therefore the use of SAMDI for quantitation. The use of a MALDI instrument capable of imaging was critical and represents the first example of iSAMDI-MS to obtain quantitative data on a large number of reactions. Each experiment required 60 nL of reagent mixture, which is nearly 200-fold less than the volume required for common multiwell plate formats. A total of 2592 reactions were simultaneously analyzed to obtain the Michaelis constant, which agreed with the value reported from batch-based methods. Important work by Gardeniers and co-workers demonstrated the benefits of combining IMS and microfluidics by quantitating 29 measurement points along the length of a serpentine, porous silicon channel to monitor arginase reaction progress.[28] Our method makes a significant advance by interfacing a 3D microfluidic device with chemically defined self-assembled monolayers to perform several thousand parallel reactions on one chip.

DOI: 10.1021/acs.analchem.8b04391
Anal. Chem. 2018, 90, 13096−13103

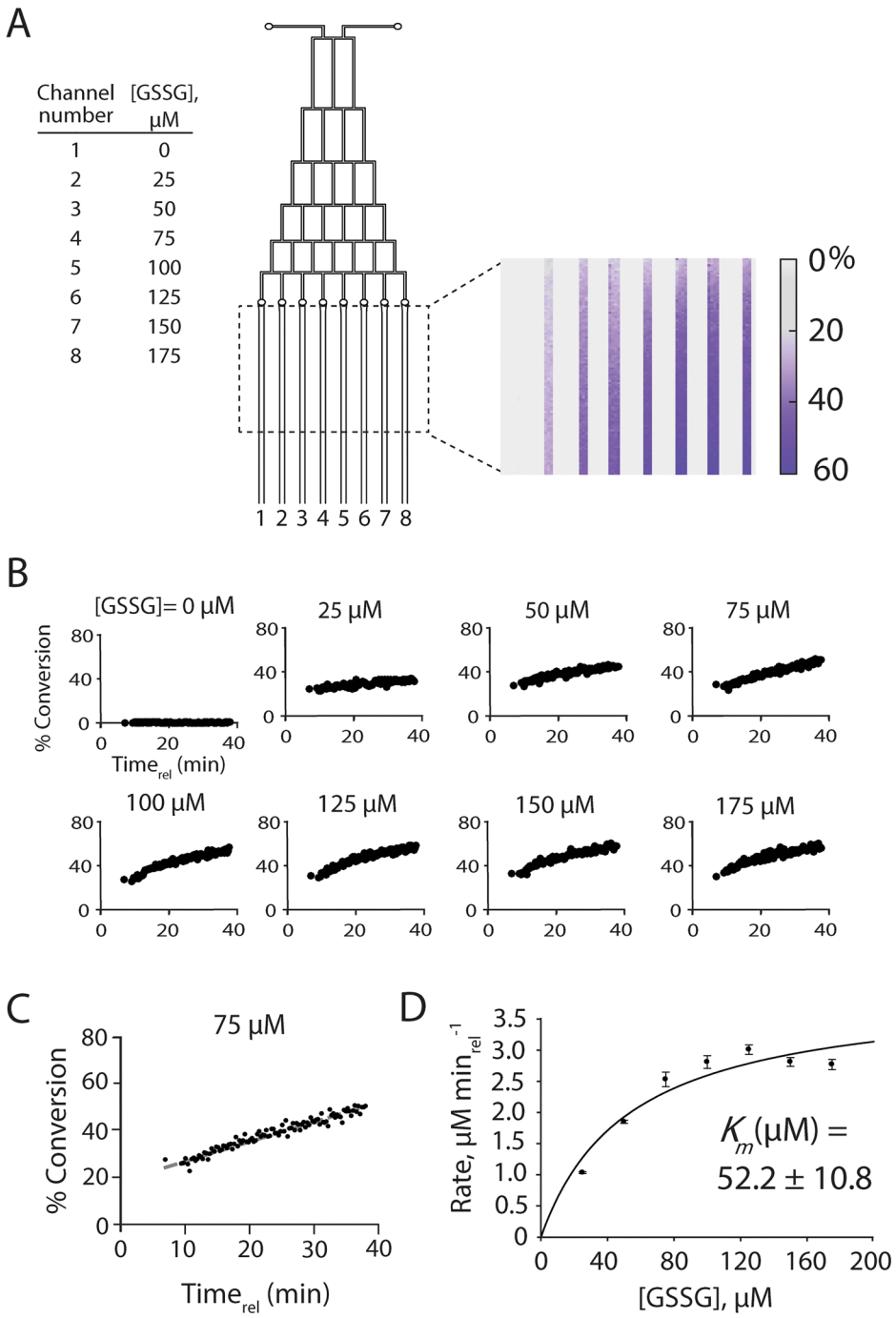

Figure 5. (A) Spatial map of hGR conversion at each *x*,*y*-coordinate (108 × 88 pixel array). (B) Representative initial velocity curves from each channel; 108 data points (pixels) each; one technical replicate. (C) Initial velocity curve from channel 4; 108 data points (pixels), R^2= 0.95. (D) Michaelis−Menten plot showing K_m= 52.2 ± 10.8 μM. Average initial velocity ($\bar{V}_0$) is calculated from three technical replicates from each channel. (Error bars) One standard deviation, three technical replicates from each channel, R^2 of 0.87.

The development of mass spectrometers with higher imaging resolution and faster scan speeds should make it possible to analyze over one million distinct reactions in one iSAMDI-MS experiment with <10 μm pixel width. Notably, Caprioli and co-workers obtained a resolution of 2.5 μm using transmission geometry MALDI-TOF-MS.[29] Commercial MALDI-IMS instrumentation can achieve lateral resolutions of approximately 10 μm and operate at laser pulse rates of 10 kHz. We recently surveyed iSAMDI-MS performance on the next generation of IMS instrumentation (rapifleX MALDI Tissuetyper, Bruker Daltonics) using the same self-assembled monolayer and matrix application methods described in this work, and we obtained comparable signal-to-noise and peak resolution at 10 μm lateral resolution. Collecting massive amounts of activity data from parallel experimentation will find useful applications in drug development, clinical diagnostic tests, directed evolution, and cellular activity assays.

Our approach uses a microfluidic device that is simple to design, fabricate, and operate. The device conducted thousands of reactions without requiring fluidic valves or isolated arrays of reaction chambers. With iSAMDI-MS, a variety of fluidic designs, ranging from the simplest single channel systems[30] to

DOI: 10.1021/acs.analchem.8b04391
Anal. Chem. 2018, 90, 13096−13103

the most complex networks,[5,31] can provide high-throughput data sets because the reaction zones are defined by the resolution of the MALDI imaging mass spectrometer. We also used 3D printing to rapidly fabricate and prototype new device designs, which can be easily adapted to other applications given the recent and widespread implementation of 3D printers in academic and commercial laboratory settings. iSAMDI-MS combines the scalability of MALDI imaging and versatility of 3D printing to greatly advance current high-throughput assay methods.

We recognize that this particular assay requires the enzyme to generate a product with a thiol available for immobilization to the maleimide groups, and that the substrate must not bind to the monolayer. Future work may generalize this assay by using chemistries that can be activated after the flow has been established at steady-state.[32−34] In this way, iSAMDI-MS might be suitable for analyzing many different types of enzymatic and chemical reactions, including those that utilize cysteine-terminated peptides,[35] thiol-terminated sugars,[36] and thiol-containing small molecules. We also emphasize that we did not measure k_{cat}, because translating a specific distance along the microfluidic channels into a reaction time is challenging due to dispersion.[37−39] Strategies to overcome dispersion might use droplets (plugs), as described by Ismagilov and co-workers,[38,40] and trapping the plugs over specific areas of the channel for subsequent reaction with the self-assembled monolayer.

The work presented here is a first example that demonstrates how iSAMDI-MS and fluidic structures can be combined to perform thousands of unique reactions from a small amount of reagents. Here, we demonstrate the measurement of a K_m value, but we expect that this method can be extended to other applications in biochemistry and chemistry.

■ ASSOCIATED CONTENT

Supporting Information

The Supporting Information is available free of charge on the ACS Publications website at DOI: 10.1021/acs.analchem.8b04391.

SolidWorks renderings of PDMS masters, % conversion, microfluidic reactor and operation, image of the chip, histogram of the diameter, plot of peak intensity, SAMDI-MS spectra, velocity curves, and peak assignments (PDF)

■ AUTHOR INFORMATION

Corresponding Author

*E-mail: milan.mrksich@northwestern.edu.

ORCID

Milan Mrksich: 0000-0002-4964-796X

Present Address

‖KCAS, LLC., 12400 Shawnee Mission Parkway, Shawnee, KS 66216, United States

Notes

The authors declare no competing financial interest.

■ ACKNOWLEDGMENTS

This material is based upon work supported by the National Science Foundation Graduate Research Fellowship under Grant DGE-1324585. In addition, the project depicted was sponsored by the Department of the Defense, Defense Threat Reduction Agency HDTRA1-15-1-0052. This work used facilities of the Northwestern University Integrated Molecular Structure Education and Research Center, the Northwestern University 3D Printing & Rapid Prototyping Lab, the Northwestern University Structural Biology Core, and the Northwestern University Research Shop - Instrumentation Design, Engineering, & Production.

■ REFERENCES

(1) Cao, Z.; Chen, C.; He, B.; Tan, K.; Lu, C. *Nat. Methods* **2015**, *12* (10), 959−962.
(2) Deshpande, S.; Dekker, C. *Nat. Protoc.* **2018**, *13* (5), 856−874.
(3) Neils, C.; Tyree, Z.; Finlayson, B.; Folch, A. *Lab Chip* **2004**, *4* (4), 342−350.
(4) Kang, D.-K.; Gong, X.; Cho, S.; Kim, J.; Edel, J. B.; Chang, S.-I.; Choo, J.; deMello, A. J. *Anal. Chem.* **2015**, *87* (21), 10770−10778.
(5) Thorsen, T.; Maerkl, S. J.; Quake, S. R. *Science* **2002**, *298* (5593), 580−584.
(6) Zheng, B.; Roach, L. S.; Ismagilov, R. F. *J. Am. Chem. Soc.* **2003**, *125* (37), 11170−11171.
(7) Boedicker, J. Q.; Li, L.; Kline, T. R.; Ismagilov, R. F. *Lab Chip* **2008**, *8* (8), 1265−1272.
(8) Hatakeyama, T.; Chen, D. L.; Ismagilov, R. F. *J. Am. Chem. Soc.* **2006**, *128* (8), 2518−2519.
(9) Grant, J.; Modica, J. A.; Roll, J.; Perkovich, P.; Mrksich, M. *Small* **2018**, *14*, 1800923.
(10) Casadonte, R.; Caprioli, R. M. *Nat. Protoc.* **2011**, *6* (11), 1695−1709.
(11) Jeon, N. L.; Dertinger, S. K. W.; Chiu, D. T.; Choi, I. S.; Stroock, A. D.; Whitesides, G. M. *Langmuir* **2000**, *16* (22), 8311−8316.
(12) Oh, K. W.; Lee, K.; Ahn, B.; Furlani, E. P. *Lab Chip* **2012**, *12* (3), 515−545.
(13) Ban, L.; Pettit, N.; Li, L.; Stuparu, A. D.; Cai, L.; Chen, W.; Guan, W.; Han, W.; Wang, P. G.; Mrksich, M. *Nat. Chem. Biol.* **2012**, *8* (9), 769−773.
(14) Berns, E. J.; Cabezas, M. D.; Mrksich, M. *Small* **2016**, *12* (28), 3811−3818.
(15) Kornacki, J. R.; Stuparu, A. D.; Mrksich, M. *ACS Chem. Biol.* **2015**, *10* (1), 157−164.
(16) O'Kane, P. T.; Mrksich, M. *J. Am. Chem. Soc.* **2017**, *139* (30), 10320−10327.
(17) Cornett, D. S.; Reyzer, M. L.; Chaurand, P.; Caprioli, R. M. *Nat. Methods* **2007**, *4* (10), 828−833.
(18) Garrett, T. J.; Prieto-Conaway, M. C.; Kovtoun, V.; Bui, H.; Izgarian, N.; Stafford, G.; Yost, R. A. *Int. J. Mass Spectrom.* **2007**, *260* (2), 166−176.
(19) Kompauer, M.; Heiles, S.; Spengler, B. *Nat. Methods* **2017**, *14* (1), 90−96.
(20) Andersson, M.; Groseclose, M. R.; Deutch, A. Y.; Caprioli, R. M. *Nat. Methods* **2008**, *5* (1), 101−108.
(21) Altelaar, A. F. M.; Taban, I. M.; McDonnell, L. A.; Verhaert, P. D. E. M.; de Lange, R. P. J.; Adan, R. A. H.; Mooi, W. J.; Heeren, R. M. A.; Piersma, S. R. *Int. J. Mass Spectrom.* **2007**, *260* (2), 203−211.
(22) Sinha, T. K.; Khatib-Shahidi, S.; Yankeelov, T. E.; Mapara, K.; Ehtesham, M.; Cornett, D. S.; Dawant, B. M.; Caprioli, R. M.; Gore, J. C. *Nat. Methods* **2008**, *5* (1), 57−59.
(23) Bokhart, M. T.; Nazari, M.; Garrard, K. P.; Muddiman, D. C. *J. Am. Soc. Mass Spectrom.* **2018**, *29* (1), 8−16.
(24) Robichaud, G.; Garrard, K. P.; Barry, J. A.; Muddiman, D. C. *J. Am. Soc. Mass Spectrom.* **2013**, *24* (5), 718−721.
(25) Henderson, G. B.; Murgolo, N. J.; Kuriyan, J.; Osapay, K.; Kominos, D.; Berry, A.; Scrutton, N. S.; Hinchliffe, N. W.; Perham, R. N.; Cerami, A. *Proc. Natl. Acad. Sci. U. S. A.* **1991**, *88* (19), 8769−8773.
(26) Becker, K.; Gui, M.; Schirmer, R. H. *Eur. J. Biochem.* **1995**, *234* (2), 472−478.

DOI: 10.1021/acs.analchem.8b04391
Anal. Chem. 2018, 90, 13096−13103

(27) Savvides, S. N.; Karplus, P. A. *J. Biol. Chem.* **1996**, *271* (14), 8101−8107.
(28) Nichols, K. P.; Azoz, S.; Gardeniers, H. J. G. E. *Anal. Chem.* **2008**, *80* (21), 8314−8319.
(29) Zavalin, A.; Yang, J.; Hayden, K.; Vestal, M.; Caprioli, R. M. *Anal. Bioanal. Chem.* **2015**, *407* (8), 2337−2342.
(30) Sengupta, S.; Dey, K. K.; Muddana, H. S.; Tabouillot, T.; Ibele, M. E.; Butler, P. J.; Sen, A. *J. Am. Chem. Soc.* **2013**, *135* (4), 1406−1414.
(31) Araci, I. E.; Quake, S. R. *Lab Chip* **2012**, *12* (16), 2803−2806.
(32) Dillmore, W. S.; Yousaf, M. N.; Mrksich, M. *Langmuir* **2004**, *20* (17), 7223−7231.
(33) Yeo, W. S.; Mrksich, M. *Adv. Mater.* **2004**, *16* (15), 1352−1356.
(34) Helal, K. Y.; Alamgir, A.; Berns, E. J.; Mrksich, M. *J. Am. Chem. Soc.* **2018**, *140* (26), 8060−8063.
(35) Wood, S. E.; Sinsinbar, G.; Gudlur, S.; Nallani, M.; Huang, C.-F.; Liedberg, B.; Mrksich, M. *Angew. Chem., Int. Ed.* **2017**, *56* (52), 16531−16535.
(36) Stenzel, M. H. *ACS Macro Lett.* **2013**, *2* (1), 14−18.
(37) Datta, S.; Ghosal, S. *Lab Chip* **2009**, *9* (17), 2537−2550.
(38) Song, H.; Chen, D. L.; Ismagilov, R. F. *Angew. Chem., Int. Ed.* **2006**, *45* (44), 7336−7356.
(39) Chen, D.; Du, W.; Liu, Y.; Liu, W.; Kuznetsov, A.; Mendez, F. E.; Philipson, L. H.; Ismagilov, R. F. *Proc. Natl. Acad. Sci. U. S. A.* **2008**, *105* (44), 16843−16848.
(40) Song, H.; Tice, J. D.; Ismagilov, R. F. *Angew. Chem., Int. Ed.* **2003**, *42* (7), 768−772.

DOI: 10.1021/acs.analchem.8b04391
Anal. Chem. 2018, 90, 13096−13103